Oncogene (2020) 39:2624–2637
https://doi.org/10.1038/s41388-020-1170-2

ARTICLE

A role for CBFβ in maintaining the metastatic phenotype of breast cancer cells

Ran Ran[1] · Hannah Harrison[1] · Nur Syamimi Ariffin[1] · Rahna Ayub[1] · Henry J. Pegg[1] · Wensheng Deng[2] · Andrea Mastro[3] · Penny D. Ottewell[4] · Susan M. Mason[5] · Karen Blyth[5,6] · Ingunn Holen[4] · Paul Shore[1]

Received: 6 June 2019 / Revised: 4 December 2019 / Accepted: 20 January 2020 / Published online: 31 January 2020

Abstract

Epithelial to mesenchymal transition (EMT) is a dynamic process that drives cancer cell plasticity and is thought to play a major role in metastasis. Here we show, using MDA-MB-231 cells as a model, that the plasticity of at least some metastatic breast cancer cells is dependent on the transcriptional co-regulator CBFβ. We demonstrate that CBFβ is essential to maintain the mesenchymal phenotype of triple-negative breast cancer cells and that CBFβ-depleted cells undergo a mesenchymal to epithelial transition (MET) and re-organise into acini-like structures, reminiscent of those formed by epithelial breast cells. We subsequently show, using an inducible CBFβ system, that the MET can be reversed, thus demonstrating the plasticity of CBFβ-mediated EMT. Moreover, the MET can be reversed by expression of the EMT transcription factor Slug whose expression is dependent on CBFβ. Finally, we demonstrate that loss of CBFβ inhibits the ability of metastatic breast cancer cells to invade bone cell cultures and suppresses their ability to form bone metastases in vivo. Together our findings demonstrate that CBFβ can determine the plasticity of the metastatic cancer cell phenotype, suggesting that its regulation in different micro-environments may play a key role in the establishment of metastatic tumours.

Introduction

The triple-negative sub-type of breast cancer is a highly aggressive cancer for which treatment options are limited [1]. Expression of the RUNX transcription factors in patients with the triple-negative sub-type of breast cancer correlates with a poor prognosis [2, 3]. Emerging evidence suggests that the role of RUNX proteins in breast cancer is dependent on the specific RUNX factor involved and the sub-type of breast cancer cell [4]. In order to consider the RUNX factors as viable targets in breast cancer therapies it is therefore critically important to determine the role of the different factors in different sub-types of breast cancer. Since CBFβ facilitates the function of all three RUNX transcription factors, establishing its role in determining the phenotype of breast cancer cells is essential [5, 6].

Mutations in CBFβ are amongst the most frequently reported for breast cancer tumours, suggesting a tumour suppressor role for CBFβ in ER+ breast cancer [7, 8]. In contrast, we and others have previously shown that expression of RUNX2 and CBFβ contribute to the metastatic phenotype of triple-negative breast cancer cells [9–12]. In this context it is therefore the maintained expression

These authors contributed equally: Ran Ran, Hannah Harrison

Supplementary information The online version of this article (https://doi.org/10.1038/s41388-020-1170-2) contains supplementary material, which is available to authorized users.

✉ Ingunn Holen
i.holen@sheffield.ac.uk

✉ Paul Shore
paul.shore@manchester.ac.uk

1 Faculty of Biology, Medicine and Health, University of Manchester, Michael Smith Building, Oxford Road, Manchester M13 9PT, UK

2 Wuhan University of Science and Technology, Jishi Rd, Hongshan Qu, Wuhan Shi, Hubei Sheng 430065, China

3 Penn State University, 428 South Frear Laboratory, University Park, Philadelphia, PA 16802, USA

4 Department of Oncology and Metabolism, University of Sheffield, Beech Hill Road, Sheffield S10 2RX, UK

5 CRUK Beatson Institute, Garscube Estate, Bearsden, Glasgow G61 1BD, UK

6 Institute of Cancer Sciences, University of Glasgow, Glasgow G61 1QH, UK

of RUNX factor activity that promotes their metastatic phenotype.

Epithelial to mesenchymal transition (EMT) contributes to the progression of metastatic cancer as it enables cancer cells to become migratory and invasive [13–15]. EMT is also a plastic programme in which cells dynamically transition along a continuum of states between epithelial and mesenchymal phenotypes [16, 17]. This plasticity is thought to enable mesenchymal cancer cells to switch from a migratory to an epithelial phenotype during colonization of the metastatic niche. Previous studies have shown that RUNX factors have different roles in EMT in different breast cell-types [18–21]. In ER-negative MCF10A cells, expression of RUNX1 suppresses EMT, whereas RUNX2 stimulates an EMT-like phenotype in these cells. In triple-negative MDA-MB-231 cells, depletion of RUNX2 inhibited their invasive capacity, consistent with suppression of EMT [22].

Since CBFβ forms functional complexes with all RUNX transcription factors, it is essential to establish its role in breast cancer metastasis. Here we show that CBFβ-depleted triple-negative cells were able to undergo a reversion from a mesenchymal phenotype to an epithelial phenotype. Indeed, acini-like structures with clear lumen were observed, reminiscent of those formed by normal epithelial breast cells. Remarkably, re-induction of CBFβ, using an inducible system, led to a complete reversion from the epithelial phenotype to a mesenchymal phenotype, demonstrating the plasticity of CBFβ-driven EMT. We subsequently show that CBFβ maintains the mesenchymal phenotype through activation of the EMT transcription factor Slug. We also show that the maintenance of the mesenchymal phenotype is dependent upon CBFβ and RUNX2, as depletion of either of these factors resulted in MET. Finally, we demonstrate that loss of CBFβ, inhibits the ability of metastatic breast cancer cells to colonise osteoblasts in long-term 3D cultures. Together our findings demonstrate that the CBFβ complexes can determine the plasticity of the metastatic cancer cell phenotype, suggesting that their regulation in different micro-environments may play a key role in the establishment of metastatic tumours.

Results

CBFβ maintains the mesenchymal phenotype of MDA-MB-231 cells

We have previously shown that depletion of CBFβ in metastatic MDA-MB-231 breast cancer cells inhibits their ability to migrate [11]. This is not restricted to MDA-MB-231 cells as knockdown of CBFβ in the MDA-MB-468 metastatic cell line also inhibited their migration (Fig. S2). We also observed that CBFβ-depleted cells exhibit a more rounded phenotype and were unable to migrate in a wound-healing assay (Fig. 1a). These observations suggested that the cells had undergone a profound phenotypic change. When grown in 3D culture, normal mammary epithelial cells differentiate into organised acini structures with clearly identifiable lumen, reminiscent of normal mammary gland morphology, whereas metastatic cells exhibit a mesenchymal phenotype and form a stellate appearance. We therefore compared the 3D morphology of wild-type metastatic breast cancer cells, MDA-MB-231, with MDA-MB-231 cells depleted of CBFβ. As expected, when grown in 3D, MDA-MB-231 cells spread throughout the culture, displaying a typical stellate pattern that reflects their mesenchymal phenotype (Fig.1b) [23]. In contrast, depletion of CBFβ resulted in a striking loss of the stellate pattern and the formation of clusters and spherical colonies (Fig. 1b).

We next used confocal microscopy to determine the extent to which the cells had differentiated in the absence of CBFβ (Fig. 1c, d). Remarkably, a small number of these structures contained clearly identifiable lumen reminiscent of acini typically formed by mammary epithelial cells (Fig. 1c–e), whilst the larger clusters did not appear to contain lumen (Fig. 1d, lower panels). Subsequent immunofluorescence staining demonstrated that some of these structures were also polarised and expressed the basement membrane markers integrins α6 and β4 on the apical surface and phospho-ezrin-radixin-moesin (pERM) on the luminal surface, as found in wild-type acini structures (Fig. 1e) [24]. These observations suggested that the cells had actually undergone a mesenchymal to epithelial transition (MET). To confirm this, we used RT-PCR to determine the expression of a number of mesenchymal and epithelial markers in wild-type MDA-MB-231 cells and the MDA-shCBFβ cells. Of the eight mesenchymal markers analysed, seven had significantly reduced expression in the MDA-shCBFβ cells. This reduction in mesenchymal markers was accompanied by an increase in expression of the four epithelial markers analysed (Fig. 1f).

Another feature of EMT is that it leads to an increase in the number of cancer stem cells (CSCs) [17]. The potential for stem cell formation can be monitored using the mammosphere assay [25]. We therefore examined the number of mammospheres formed in the presence and absence of CBFβ. Loss of CBFβ resulted in a significant reduction in the number of mammospheres formed when compared to parental MDA-MB-231 cells, suggesting that in the absence of CBFβ the potential to produce CSCs is reduced (Fig. 1g). Taken together, our data demonstrate that CBFβ is essential for the maintenance of the mesenchymal phenotype in MDA-MB-231 cells and suggests that loss of CBFβ expression causes differentiation towards a more epithelial-like phenotype.

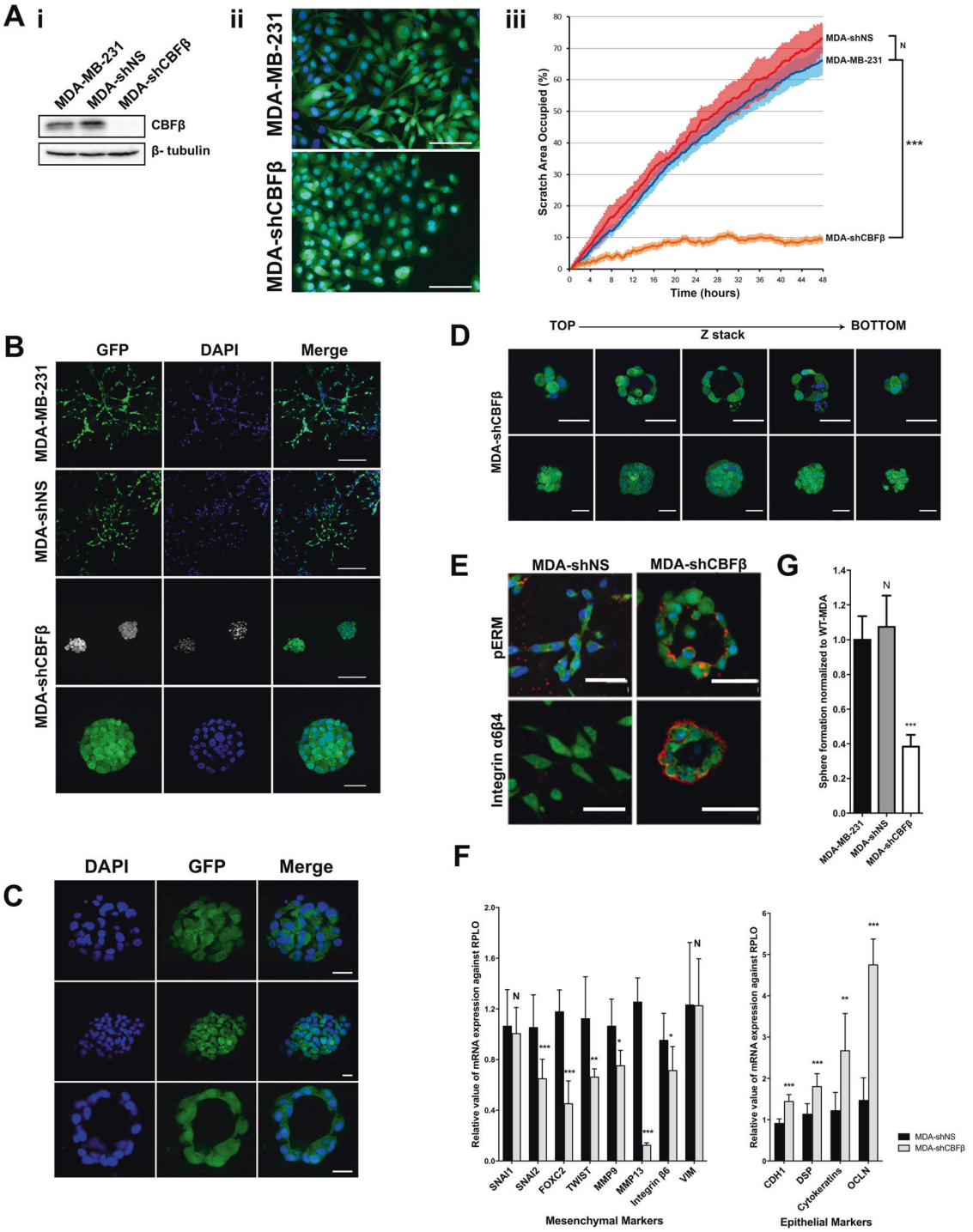

Examination of EMT marker expression in MDA-MB-468 cells in the absence of CBFβ showed that the mesenchymal markers SNAI2 and OPN increased significantly, with little change in other mesenchymal markers, including MMP9, SNAI1 and Vimentin. MMP13 was the only mesenchymal marker examined that displayed a reduction in expression. Expression of the epithelial markers cytokeratin-7, desmoplakin and E-cadherin did not change either. These data show that CBFβ is required to maintain the invasive capacity of MDA-MB-468 cells but its loss does not result in a complete MET, as determine by the limited changes in classical EMT marker gene expression. When compared with MDA-MB-231 cells these findings suggest that both cell-types require CBFβ for invasion but that it is likely that RUNX complexes regulate different gene expression programmes dependent on the

◀ **Fig. 1 CBFβ maintains the mesenchymal phenotype of metastatic breast cancer cells. a** CBFβ loss results in phenotypic changes. (i) Western blot shows knockdown of CBFβ in MDA-MB-231 cells, MDA-shNS and MDA-shCBFβ. The two CBFβ bands likely correspond to the two isoforms known to form complexes with RUNX proteins, CBFβ (p22) and CBFβ (p21.5). It is likely that the two bands correspond to these isoforms as they have similar molecular weights. β-Tubulin was used as a loading control. (ii) Fluorescent microscopy comparing the shape of GFP-expressing MDA-MB-231 cells and CBFβ-depleted cells (MDA-shCBFβ). (iii) Following scratch of a monolayer, live images were taken every 20 min for 48 h. Graph shows significant reduction in cell mobility in the absence of CBFβ. Statistical analysis performed using ANOVA. **b** Loss of CBFβ results in cluster formation in 3D culture. MDA-MB-231, MDA-shNS and MDA-shCBFβ were grown in 3D Matrigel for 14 days. GFP (green) was stably expressed in all cell lines. Cells were fixed and nuclei stained with DAPI (blue). The wild-type and MDA-shNS cells showed a stellate mesenchymal growth pattern whilst MDA-shCBFβ cells formed discrete clusters. Scale bars are 200 µm in the top three rows and 50 µm in row four. (**c**) Confocal microscopy showing different sizes of clusters in the MDA-shCBFβ cells. The lower panels clearly show a smaller cluster that resembles an acinus. Scale bars are 25 µm. **d** Z-stack analysis showing that some smaller clusters contain lumen and some do not. Scale bars are 50 µm. **e** Acini express polarity markers. Immunofluorescence microscopy of MDA-shNS and MDA-shCBFβ cells in 3D Matrigel after 14 days. Cells were fixed and stained for apical or basement markers including phospho-Ezrin/Radixin/Moesin (pERM) and Integrins (Red) and nuclei were stained with DAPI (Blue). Scale bars are 50 µm. **f** Loss of CBFβ causes a reduction in mesenchymal markers and increased expression of epithelial markers. qRT-PCR was performed for epithelial and mesenchymal markers in MDA-shNS or MDA-shCBFβ from cells grown in 2D culture. **g** Loss of CBFβ causes a reduction in the number of mammosphere-forming colonies. Mammospheres were counted after 5 days growth in non-adherent culture.

specific cellular context. Our subsequent analysis therefore focussed on the role of CBFβ and RUNX transcription factors in EMT/MET transition in MDA-MB-231 cells.

CBFβ regulates EMT/MET state-transition

Dynamic EMT/MET state-transition is thought to enable metastatic cancer cells to switch between the two phenotypes, a property that allows them to both invade and colonise other tissues [17, 26]. We therefore sought to establish if the dynamic EMT/MET state-transition could be regulated by the expression of CBFβ. To do this we created a cell line in which the activity of CBFβ can be regulated by the addition of 4-Hydroxytamoxifen (4OH-T) (Fig. 2a) [27]. MDA-shCBFβ cells stably expressing a CBFβ-ER fusion protein were generated and western blotting confirmed that the addition of 4OH-T to these cells induced nuclear expression of CBFβ-ER (Fig. 2a). RT-PCR analysis showed that there was also a concomitant increase in expression of the known RUNX-target genes OPN, MMP9 and MMP13 (Fig. 2b). Activation of CBFβ also rescued the migration defect, as determined by a significant increase in the capacity of the cells to invade Matrigel and migrate in a wound-healing assay in the presence of 4OH-T (Fig. 2c). Microscopic analysis of the cells in 3D culture, in the presence and absence of 4OH-T, revealed a remarkable difference in phenotypes. In the absence of 4OH-T the cells formed clusters as expected (Fig. 2d, upper panel). However, cells grown in the presence of 4OH-T had spread throughout the culture and were indistinguishable from the parental MDA-MB-231 cells (Fig. 2d and see Fig. S3 for controls). Furthermore, activation of CBFβ induced an increase in expression of mesenchymal markers and a decrease in epithelial markers (Fig. 2e). Consistent with this, we observed an increase in the number of mammospheres formed following culture with 4OH-T (Fig. 2f). To demonstrate that CBFβ can dynamically regulate the plasticity of the cells we added 4OH-T to MDA-CBFβ-ER cells that had already formed clusters in 3D culture (Fig. 2g). In the absence of 4OH-T the clusters continued to grow with little dispersion. In contrast, after three days in the presence of 4OH-T branched structures were observed, and after 6 days cells were clearly dispersing (Fig. 2g). These data show that CBFβ drives the mesenchymal phenotype of MDA-MB-231 and that the EMT/MET state-transition can be dynamically regulated in metastatic cells by CBFβ.

Depletion of RUNX1 and RUNX2 induces MET

Since both RUNX1 and RUNX2 are expressed in MDA-MB-231 cells, we sought to establish if a double knockdown of RUNX1 and RUNX2 phenocopied the effect of CBFβ-knockdown. We therefore generated cell lines in which either RUNX1 or RUNX2 were depleted and a cell line in which both proteins were depleted (Figs. 3a, S4A and S5A). All three cell lines displayed a significant decrease in migration and invasion capacity (Figs. 3b, c, S4 and S5) as well as a decrease in mammosphere formation (Figs. 3d, S4 and S5). Mesenchymal and epithelial marker expression confirmed that each of the knockdown cell lines had undergone MET (Figs. 3e, S4 and S5). All of the lines formed clusters in 3D culture (Figs. 3f, S4 and S5). In addition, we observed acini-like structures in the double knockdown cells demonstrating that depletion of both proteins does indeed phenocopy the effect of CBFβ loss (Fig. 3f). We did not observe acini in the single knockdown cell lines, although acini-like structures have previously been reported in RUNX2-knockdown cells [22]. Taken together, these findings demonstrate that CBFβ, RUNX1 and RUNX2 are necessary for the maintenance of the mesenchymal phenotype in MDA-MB-231 cells.

RUNX/CBFβ drives Slug expression to maintain EMT

The EMT transcription factor Slug is encoded by the SNAI2 gene whose expression is reduced in CBFβ, RUNX1 and

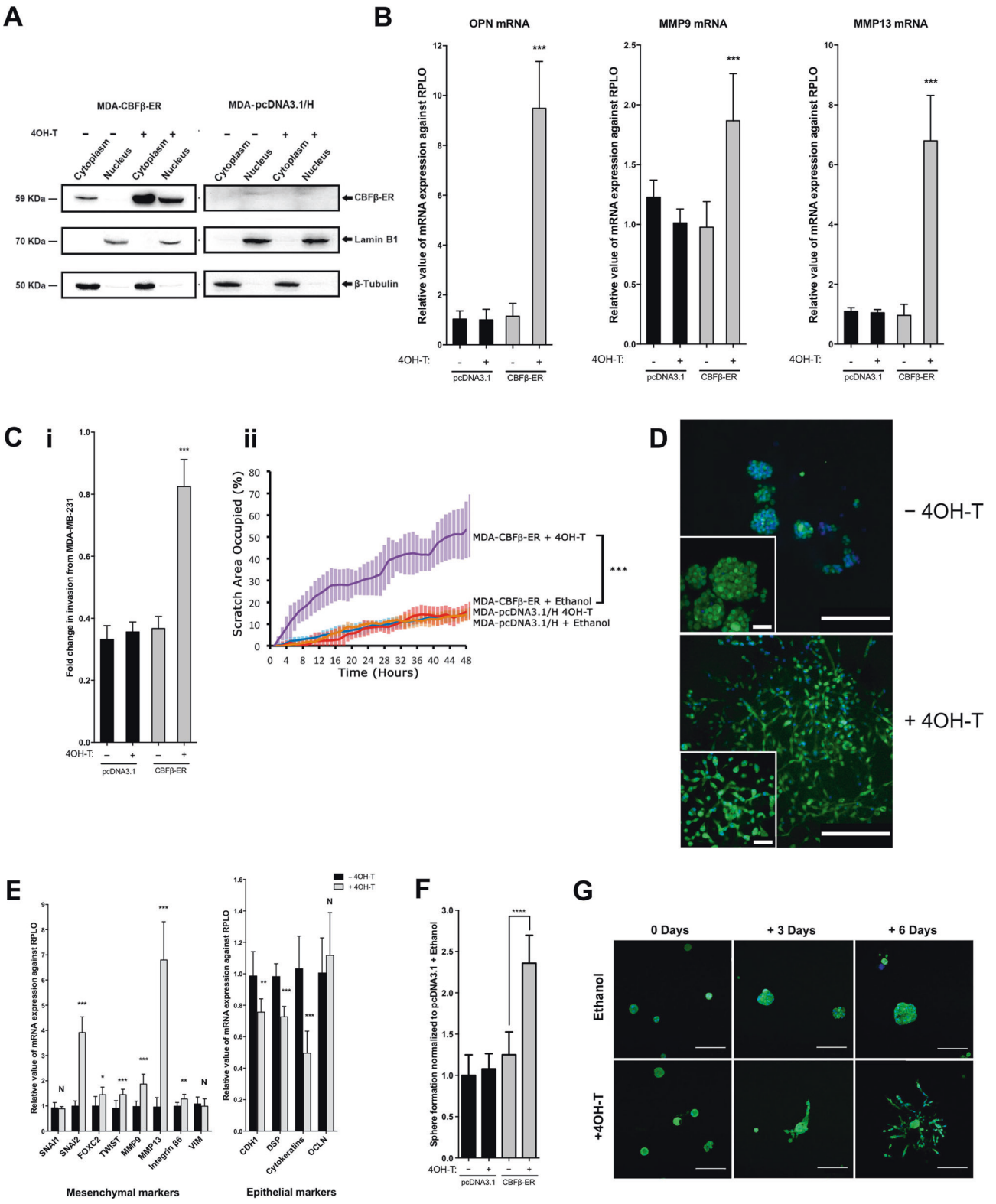

RUNX2-knockdown cell lines (Figs. 1f, S4 and S5) [16, 18]. To confirm that the changes in SNAI2 mRNA expression correlated with Slug protein expression we used western blotting to determine Slug expression in the MDA-CBFβ-ER cell line in the presence and absence of 4OH-T (Fig. 4a). In the absence of 4OH-T Slug expression was significantly reduced whereas addition of 4OH-T resulted in a clear increase in expression (Fig. 4a). This suggested that

◀ **Fig. 2 CBFβ regulates EMT/MET state-transition. a** Inducible activation of CBFβ. Western blots showing nuclear and cytoplasmic extracts from 4OH-T and ethanol treated MDA-CBFβ-ER cells using anti-CBFβ antibody. Lamin B1 and Tubulin were used as nuclear and cytoplasmic loading controls, respectively. **b** RUNX-target genes are activated in MDA-CBFβ-ER cell lines by 4OH-T. Total RNAs were used to analyse the mRNA levels of known RUNX-target genes, OPN (osteopontin), MMP9 (matrix metallopeptidase-9) and MMP-13 (matrix metallopeptidase-13). **c** Activation of CBFβ-ER with 4OH-T restores cell invasion and mobility capacity. (i) Matrigel invasion assay showing the recovery of invasion in the presence of 4OH-T following 24 h culture. (ii) Following scratch of a monolayer, live images were taken every 20 min for 48 h. Graph shows migration capacity is restored in the presence of 4OH-T in CBFβ-ER cells. Statistical analysis performed using ANOVA. **d** Induction of CBFβ-ER with 4OH-T restores the mesenchymal phenotype in 3D culture. The GFP-expressing cells were visualised by fluorescence microscopy and DAPI staining. The upper panel shows MDA-CBFβ-ER cells grown after addition of vehicle (ethanol). The lower panel shows 4OH-T treated MDA-CBFβ-ER cells. Scale bars are 200 μm in the large image and 50 μm in the inset image. **e** Re-expression of CBFβ restores EMT marker gene expression. Epithelial and mesenchymal marker genes were analysed by qRT-PCR on RNA isolated from MDA-CBFβ-ER cells grown in the presence 4OH-T or ethanol. **f** Induction of CBFβ-ER restores mammosphere formation capacity. MDA-CBFβ-ER and control MDA-pcDNA3.1/H cells were grown with 4OH-T or ethanol and their mammopshere forming capacity subsequently determined. Mammospheres were counted after 5 days growth in non-adherent culture. **g** Immunofluorescence microscopy of MDA-CBFβ-ER cells in 3D culture showing dispersion of cell clusters upon activation of CBFβ. Cells were grown in Matrigel for 8 days (day 0 of 4OH-T addition), prior to addition of 4OH-T or ethanol. Cells were fixed and visualised for GFP (green) and DAPI (blue). Scale bars are 200 μm.

the reduction in Slug expression in CBFβ-depleted cells contributes to the loss of the observed EMT. To test this, we predicted that re-expression of Slug should rescue the migration phenotype of CBFβ-depleted cells. We therefore generated a cell line stably expressing Slug in the CBFβ-depleted cells. Analysis of these cells in the wound-healing assay revealed that their ability to migrate had significantly recovered (Fig. 4b). Moreover, these cells exhibited a stellate phenotype reminiscent of the wild-type MDA-MB-231 cells, when grown in 3D culture (Fig. 4c, lower panels). Furthermore, Slug was depleted in the RUNX1/2-knockdown cell line and their migratory phenotype was rescued by the ectopic expression of Slug (Fig. 4d). ChIP analysis of the SNAI2 promoter clearly demonstrated that both RUNX1 and RUNX2 could immunoprecipitate the promoter but not a control sequence 1.5 kb upstream (Fig. 4e). Binding to the promoter was abrogated in RUNX1 and RUNX2-depleted cells (Fig. 4e). Taken together, these data demonstrate that the RUNX/CBFβ complexes maintain the mesenchymal phenotype of MDA-MB-231 cells, at least in part, by regulating the expression of the EMT transcription factor Slug.

CBFβ contributes to the development of bone metastasis in mice

To investigate the metastatic potential of the CBFβ-depleted cells, we first determined their tumourigenic capacity by direct transplant into the mammary fat pad of mice (Fig. 5a) [28]. Numbers of tumours in both control and CBFβ-depleted cells were similar, however tumour volume in the CBFβ-depleted cells was significantly less than the shNS cells (Fig. 5a). This correlated with the slower growth rate of these cells observed in 3D culture (Fig. 5b). To determine if the MET induction caused by the loss of CBFβ affected the ability of cells to invade a metastatic niche we first compared the growth of parental MDA-MB-231 cells with the CBFβ-depleted cells in co-cultures with osteoblasts which had been growing for 12 weeks in 3D (Fig. 5c) [29]. Eight days after adding the cells to the osteoblast cultures, the GFP-expressing parental cells had invaded throughout the culture, whereas the CBFβ-depleted cells formed discrete clusters and did not permeate the osteoblast network (Fig. 5c). Having established that the CBFβ-depleted cells retain the ability to form localised tumours but have a restricted capacity to grow in osteoblast culture, we next tested their ability to establish bone metastases after injection into the circulation by intracardiac injection (Fig. 5d) [30]. Initial experiments with the CBFβ-depleted cells resulted in bone tumours in which CBFβ-expression had recovered from the shRNA (data not shown). This observation suggested that CBFβ was indeed required for bone metastases to form. We therefore created a CBFβ-depleted cell line using CRISPR-Cas9 (Figs. 5d, S6) [31]. These $CBF\beta^{-/-}$ cells showed the same loss of mesenchymal phenotype, decreased invasion, mammosphere formation and mesenchymal markers as seen in the shCBFβ cells (Fig. S6). Intracardiac injection of the CBFβ-CRISPR cells into mice resulted in a striking reduction of the number of mice developing bone tumours compared with controls (Fig. 5d). We found that 7 out of 11 animals injected with the control cells developed tumours in the hind limbs, with numerous cancer-induced bone lesions detected, compared with three out of seven animals injected with CBFβ-CRISPR (Fig. 5d). In addition, the animals receiving the control cells had higher numbers of skeletal lesions (average = 8.1 lesions/mouse) compared with those receiving CBFβ-CRISPR cells (average = 1.7 lesions/mouse), (Fig. 5d). These data demonstrate that loss of CBFβ reduces the ability of MDA-MB-231 cells to metastasise to bone.

Discussion

In this study, we have shown that the RUNX co-regulator CBFβ is essential to drive MDA-MB-231 breast cancer cells

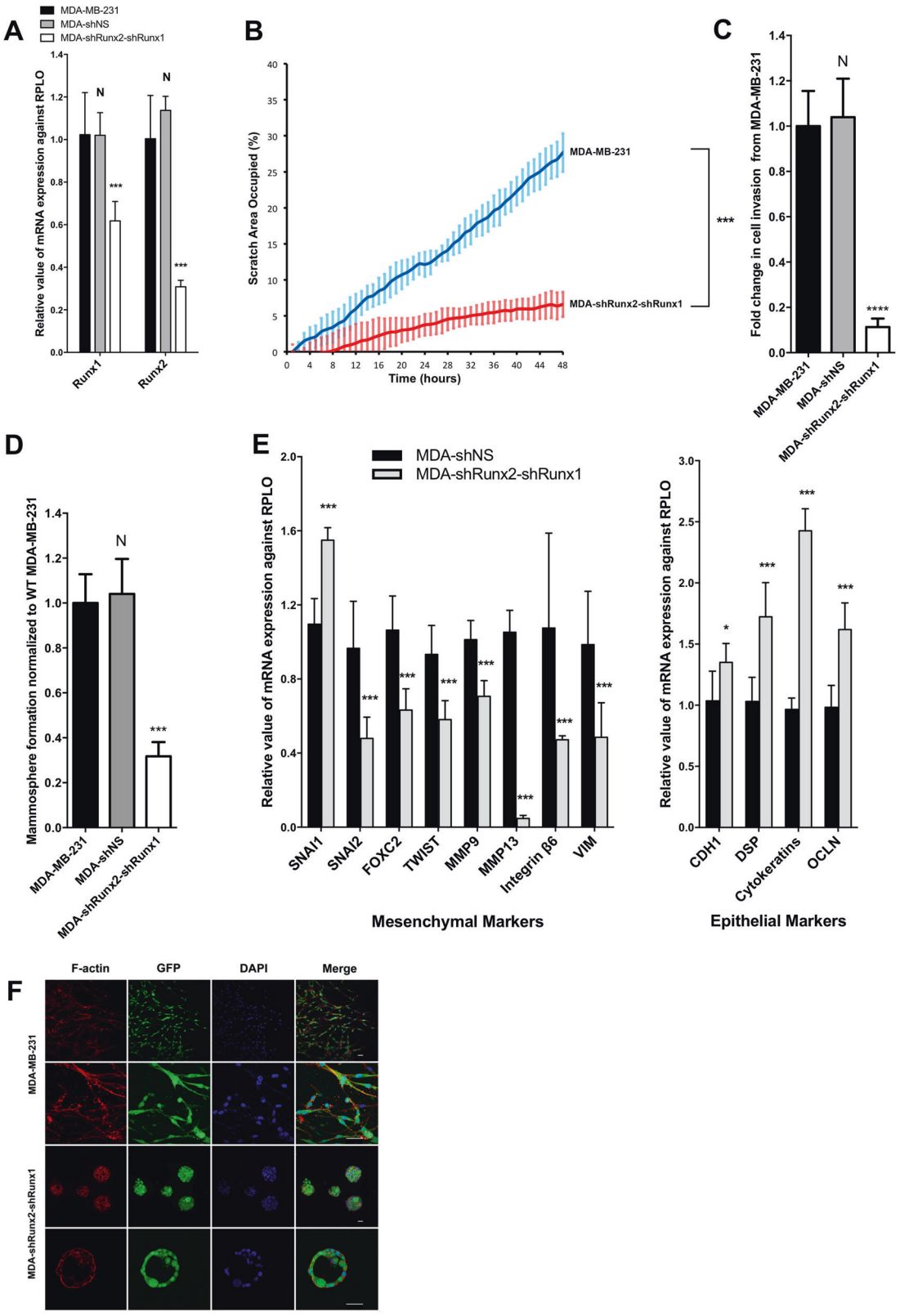

through EMT. Maintenance of the mesenchymal phenotype is, at least in part, achieved by regulating the expression of the EMT transcription factor Slug. We also demonstrated that the MET induced by loss of CBFβ is completely reversible by re-expression of CBFβ. These findings are important since they demonstrate that, in principle,

◀ **Fig. 3 Knockdown of RUNX1 and RUNX2 induces MET. a** qRT-PCR showing knockdown of RUNX1 and RUNX2 by shRNA. Total RNAs were used to analyse the mRNA levels of RUNX1 and RUNX2. RPLO mRNA was used as a control for normalisation and relative values are shown. **b** Scratch assays showing inhibition of migration in MDA-shRUNX2-shRUNX1 cells. Following scratch of a monolayer, live images were taken every 20 min for 48 h. Graph shows significant reduction in cell mobility in the absence of RUNX1/RUNX2. **c** Matrigel invasion assay showing inhibition of migration in MDA-shRUNX2-shRUNX1 cells. **d** Loss of RUNX1 and RUNX2 causes a reduction in mammosphere formation. Mammospheres were counted after 5 days growth in non-adherent culture. **e** Loss of RUNX1 and RUNX2 in MDA-MB-231 cells causes a reduction in mesenchymal markers and increased expression of epithelial markers as seen by RT-PCR. **f** Loss of RUNX1 and RUNX2 results in cluster formation in 3D culture. Immunofluorescence microscopy of MDA-MB-231 and MDA-shRUNX2-shRUNX1 cells in Matrigel after 14 days growth. The confocal images show equatorial cross sections. Scale bars are 50 μm.

regulation of RUNX/CBFβ activity can determine the extent to which triple-negative breast cancer cells differentiate along the epithelial-mesenchymal continuum. In the context of metastasis in vivo this raises the possibility that interactions between cancer cells and the microenvironment influence the activity of RUNX/CBFβ, thereby shifting their phenotype toward the epithelial state and enabling the cells to colonise the new niche. Indeed, the loss of CBFβ significantly reduced the capacity of metastatic cancer cells to invade osteoblast cultures in vitro and to form osteolytic lesions in vivo.

Previous work has shown that about two thirds of the RUNX1 transcriptome is shared with the RUNX2 transcriptome in MCF7 cells [19]. Our finding that CBFβ, RUNX1 and RUNX2 are all necessary for SNAI2 expression suggests that all three factors combine to ensure a sufficient level of Slug is available to maintain the mesenchymal phenotype. This suggests that none of these factors are redundant in this context. This may reflect the need for a threshold level of RUNX factors to be expressed but does not discount the possibility that RUNX1 and RUNX2 also regulate specific subsets of genes. SNAI2 is a well-established EMT transcription factor that appears to be a key target for RUNX transcription factor complexes and is perhaps one of several genes that contribute to the metastatic nature of breast cancer cells [16, 18].

In contrast to these findings, we did not observe significant changes in classical EMT markers when either CBFβ or RUNX1 was depleted in MDA-MB-468 cells. The emerging picture is that RUNX complexes have pleiotropic effects dependent on the cellular context and it is of note that whilst MDA-MB-231 and MDA-MB-468 cells are both "triple-negative" they exhibit different characteristics and gene expression profiles, MDA-MB-231 being of the claudin low sub-type and MDA-MB-468 are basal [32]. Moreover, mutations in RUNX1 and CBFβ are associated with the ER+ sub-type of breast cancer and is therefore predicted to have a tumour suppressor role in this context [7, 8, 33]. Indeed, previous studies have shown that RUNX1 suppresses development of ER+ luminal breast cancer but it is not known how CBFβ contributes in this context [34]. Our finding that depletion of RUNX1 in MDA-MB-231 cells induces MET is in agreement with a previous study in which the expression of miR-378 in MDA-MB-231 cells, which inhibits RUNX1 expression, also resulted in suppression of migration and invasion [35]. However, this is in contrast to the role of RUNX1 in MCF10A and MCF7 cells where RUNX1 expression is required to maintain an epithelial-like phenotype [20, 36]. Taken together these findings suggest that RUNX transcription factors contribute to the epithelial-mesenchymal continuum is a cell-context dependent manner.

Finally, small molecule inhibitors that inhibit the interaction between CBFβ and RUNX have been shown to inhibit colony formation in a basal-like breast cancer cell line [37]. Our findings that CBFβ is essential to maintain the mesenchymal phenotype, and that it contributes to the formation of bone metastases, suggests that in principle inhibiting this complex might maintain metastatic colonies in a less aggressive epithelial state by driving MET. Thus, targeting the RUNX/CBFβ complex in this way might be a viable option to treat a sub-group of triple-negative breast cancer patients.

Methods

Cell lines

Parental MDA-MB-231 expressing GFP were a kind gift from D. Welch, University of Alabama. MDA-MB-231-shCBFβ/RUNX1/RUNX2 were produced using Sure Silencing shRNA plasmids (SABiosciences) as previously described [16]. Lines were authenticated by multiplex-PCR assay using the AmpF/STR system (Applied Biosystems) and confirmed as mycoplasma free. Monolayers were grown in complete medium (DMEM/10% FCS/2 mmol/L L-glutamine/PenStrep 0.4 μg/mL puromycin, 50 μg/mL geneticin, 500 μg/mL hygromycin as required) and maintained in a humidified incubator at 37 °C at an atmospheric pressure of 5% (v/v) CO_2/air.

Western blotting

Protein was separated on an SDS–PAGE and transferred to Hybond-C Extra nitrocellulose membrane. Primary antibodies included: β-Tubulin (Abcam, ab6046), Lamin-B1 (Abcam, ab16048), CBFβ (Abcam, ab33516), RUNX1 (Abcam, ab23980), RUNX2 (MBL, D130-3), Snai2 (Cell Signalling, C19G7), FLAG (Sigma, F1804).

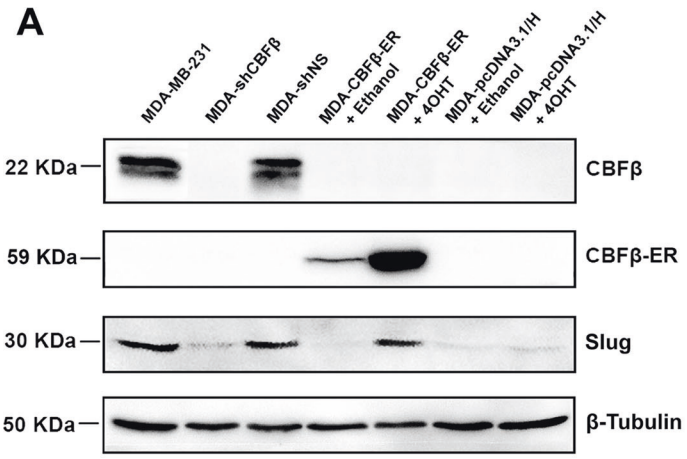
A
MDA-MB-231
MDA-shCBFβ
MDA-shNS
MDA-CBFβ-ER + Ethanol
MDA-CBFβ-ER + 4OHT
MDA-pcDNA3.1/H + Ethanol
MDA-pcDNA3.1/H + 4OHT
22 KDa
CBFβ
59 KDa
CBFβ-ER
30 KDa
Slug
50 KDa
β-Tubulin

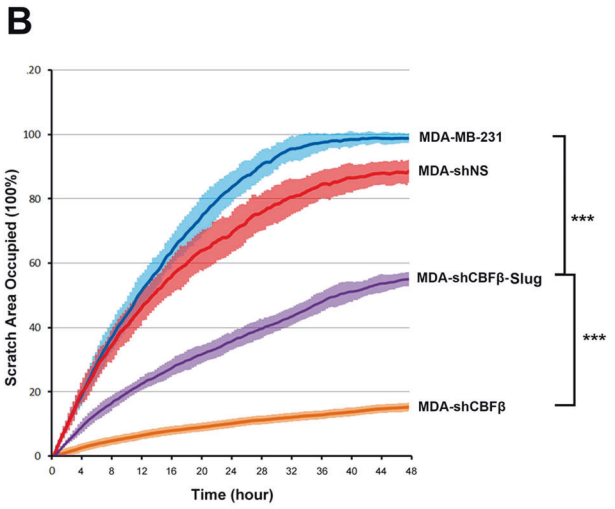
B
Scratch Area Occupied (100%)
Time (hour)
MDA-MB-231
MDA-shNS
MDA-shCBFβ-Slug
MDA-shCBFβ
***
***

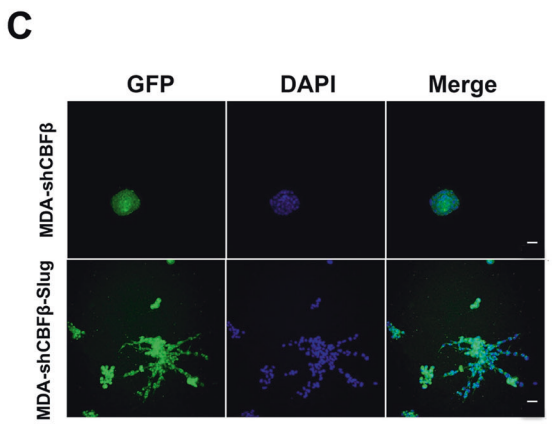
C
GFP
DAPI
Merge
MDA-shCBFβ
MDA-shCBFβ-Slug

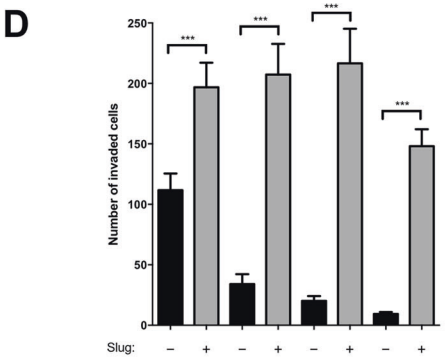
D
Number of invaded cells
Slug:

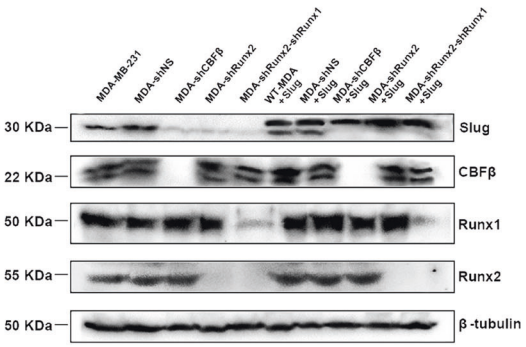
MDA-MB-231
MDA-shNS
MDA-shCBFβ
MDA-shRunx2
MDA-shRunx2-shRunx1
WT-MDA +Slug
MDA-shNS +Slug
MDA-shCBFβ +Slug
MDA-shRunx2 +Slug
MDA-shRunx2-shRunx1 +Slug
30 KDa
Slug
22 KDa
CBFβ
50 KDa
Runx1
55 KDa
Runx2
50 KDa
β-tubulin

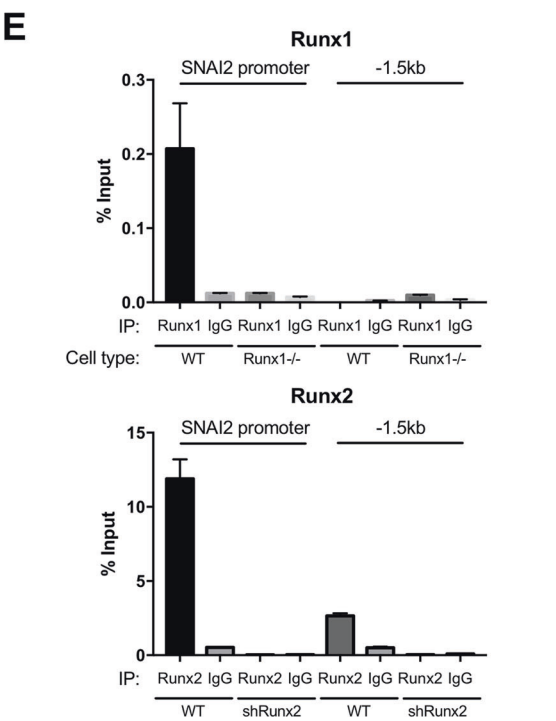
E
Runx1
SNAI2 promoter
-1.5kb
% Input
IP:
Cell type:
WT
Runx1-/-
Runx2
shRunx2

◀ **Fig. 4 RUNX/CBFβ maintains EMT via the EMT transcription factor Slug. a** Activation of CBFβ restores expression of Slug in MDA-CBFβ-ER cells. Western blot for CBFβ and Slug performed on cell lysates from MDA-MB-231, MDA-shCBFβ, MDA-shNS, MDA-CBFβ-ER and MDA-pcDNA3.1/H cells in the presence and absence of 4OH-T. Tubulin was used as the loading control. **b** Slug expression in MDA-shCBFβ cells partially restores cell migration capacity. Wound-healing assay showing the recovery of migration capacity in cell depleted of CBFβ and cells stably expressing Slug. Following scratch of a monolayer, live images were taken every 20 min for 48 h. **c** Re-expression of Slug induces a mesenchymal spreading phenotype in MDA-shCBFβ cells in 3D culture. Scale bars are 50 µm. **d** Expression of Slug in RUNX-depleted cells restores their invasive capacity. Cells were transfected with a Slug-Myc expressing plasmid or the control plasmid pcDNA3.1/Hygro. Western analysis shows expression of exogenous Slug-Myc. Expression of endogenous Slug (lower band in the Slug panel) and exogenous Slug-Myc (upper band in the Slug panel) was analysed by western blot from total cell lysates 72 h after transfection. The Graph shows Matrigel invasion assays of transiently transfected Slug-Myc-expressing cells. Invasion was restored in all three knockdown cells (from left to right, MDA-shNS, MDA-shCBFβ, MDA-shRunx2, MDA-shRunx2-shRunx1 cells). **e** ChIP assay showing binding of RUNX1 and RUNX2 to the SNAI2 promoter. Percentage input of RUNX protein binding is shown relative to the anti-rabbit IgG antibody.

For all experiments three biological replicates were performed and densitometry was conducted to calculate average changes using ImageJ software, which is freely available at http://rsb.info.nih.gov/ij/.

Cell scratch assay

Confluent monolayers were scratched on day 0 and medium was changed to serum free. Cells were grown in an AS MDW live cell imaging microscope system at 37 °C 5% CO_2 for 48 h. Images were taken every 20 min and 40 views were taken in each well. For all experiments three technical and three biological replicates were performed. Image data analysis was performed using Cell Profile software.

Overlay three-dimensional culture of breast cells

Matrigel (Corning, 354230) was thawed on ice overnight at 4 °C and then spread evenly onto dishes (MatTek P35G-1.0-14-C) or into 24-well plates (Greiner, Bio-one 662892). Cells were resuspended in 3D assay medium (2% Matrigel, 95% DMED, 2%FBS, 1% Pen/Strep, 1% nonessential amino acid, 1% L-glutamine) and plated on to solidified Matrigel. Cells were grown in 5% CO_2 humidified incubator at 37 °C. Assay medium was changed every 3 or 4 days. Cells were fixed at day 14. For all experiments three technical and three biological replicates were performed.

Microscopy

2D culture

Images were collected on a Zeiss Axioimager.D2 upright microscope using a 10× objective and captured using a Coolsnap HQ2 camera (Photometrics) through Micromanager software v1.4.23. Specific band pass filter sets for DAPI, FITC and Cy5 were used to prevent bleed through from one channel to the next.

3D culture

Images were collected on a Leica TCS SP5 AOBS inverted and upright confocal microscopes. Images were collected using PMT detectors with the following detection mirror settings; [FITC 494–530 nm; Texas red 602-665 nm; Cy5 640-690 nm] using the [488 nm (20%), 594 nm (100%) and 633 nm (100%)] laser lines, respectively. When it was not possible to eliminate cross-talk between channels, the images were collected sequentially. When acquiring 3D optical stacks the confocal software was used to determine the optimal number of Z sections. Only the maximum intensity projections of these 3D stacks are shown in the results. Images were then processed and analysed using Fiji ImageJ (http://imagej.net/Fiji/Downloads) [14], which is freely available online.

For all experiments three technical and three biological replicates were performed.

Immunofluorescence

For cell grown on coverslips, fixing and permeabilisation was performed in 4% paraformaldehyde (Sigma) and 0.1% Triton-100 (Sigma) before blocking in 1% Bovine Serum Albumin. The cells were then incubated with the primary antibodies overnight at 4 °C at a dilution of 10 µg/µl). pERM (Cell Signalling Technology; Antibody #3141), anti-integrin avβ6 (Abcam, ab97588). Alexafluor secondary antibodies (Invitrogen) were used at a 1/200 dilution. The coverslips were mounted on glass slides using mounting medium with DAPI (Invitrogen P36965). For cells grown in Matrigel, following fixing and permeabilisation as detailed above non-specific staining was blocked using cells were blocked using IF Buffer (7.7 mM NaN3, 0.1% bovine serum albumin, 0.2% Triton X-100, 0.05% Tween-20 in PBS) + 10% goat serum. Cells were stained using Phalloidin for F-actin (Sigma, P1951) and mounted using DAPI (Invitrogen).

For all experiments three technical and three biological replicates were performed.

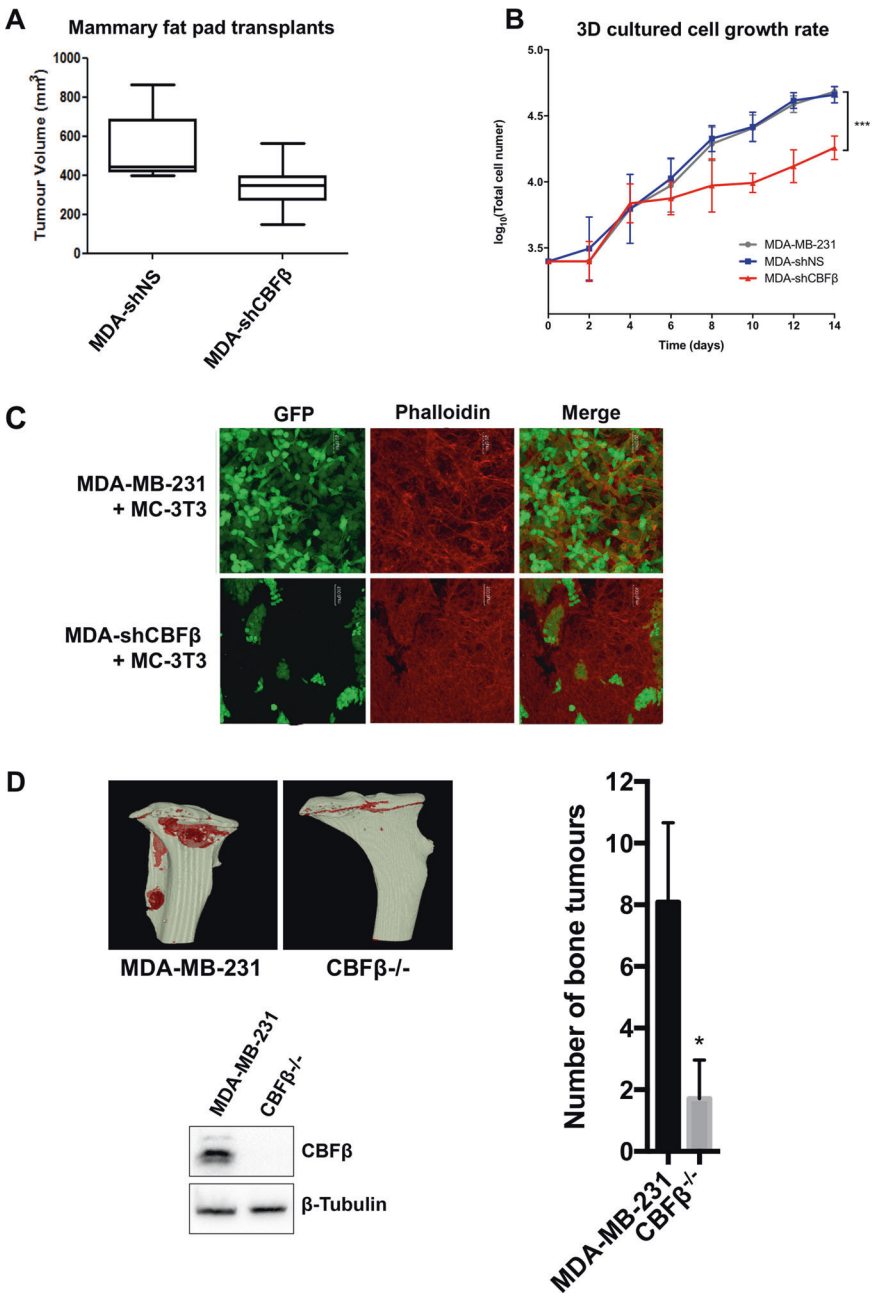

Fig. 5 CBFβ contributes to the development of bone metastasis. a MDA-MB-231 cells were transplanted into the inguinal mammary fat pad of *CD1-Nude* females. Data shown at 4 weeks post-transplantation. Data is presented as mean ± SDM (shNS; $n = 5$; shCBFβ; $n = 7$). The difference between the two groups is significant ($p < 0.05$) as determined using an unpaired Student's *t*-test. **b** Growth curves showing knockdown of CBFβ reduces growth rate in 3D culture. MDA-MB-231, MDA-shNS, or MDA-shCBFβ cells were grown on 3D culture and cells were counted every 2 days. **c** Knockdown of CBFβ inhibits invasion in 3D co-cultures with osteoblasts. 3D cultures of MC-3T3 osteoblasts were grown for 2 months prior to addition of MDA-MB-231 or MDA-shCBFβ cells. Confocal images were taken after 8 days of co-culture. Cells were stained with phalloidin. MDA cells were identified by GFP fluorescence. **d** CBFβ silencing reduces tumour growth in bone in vivo. MDA-MB-231 control or CBFβ$^{-/-}$ cells were injected i.c. into 6-week old BALB/c nude mice and tumour growth in the hind limbs analysed 26 days later. 3D reconstruction of tumour-bearing tibia showing the presence of osteolytic lesions. The histogram shows the average number of bone tumours per mouse for each cell line as indicated.

Mammosphere culture

Mammosphere culture was carried out as previously described [38]. Spheres >50 μm were counted on day 5. For all experiments three technical and three biological replicates were performed.

Quantitative reverse transcription PCR

RNA was extracted using the Qiagen RNAeasy kit according to manufacturer's instructions and quantified on the Nanodrop spectrophotometer (Thermo). Real time one step qRT-PCR was carried out using the QuantiTect SYBR® Green RT-PCR Kit (Qiagen) according to manufacturer's instructions before analysis on the 7900 PCR machine (Applied Biosystems). A table of the primers used can be found in Supplementary Table 1. For all experiments three biological replicates were performed.

Inducible Cell line production

Mouse CBFβ-FLAG and ER was ligated into pcDNA3.1/Hygro(-) vector producing pcDNA3.1/Hygro(-)-CBFβ-FLAG-ER. Stable lines were made using this vector and cells were

transfected using Lipofectamine according to manufacturer's instructions (Fig. S1).

Nuclear/Cytoplasmic separation

Cells were resuspended in 400 µl of ice cold Buffer A (10 mM HEPES pH 7.9, 10 mM KCl, 0.1 mM EDTA, 0.1 mM EGTA, 1 mM DTT, 0.5 mM PMSF) with the addition of complete mini-EDTA-free protease inhibitor cocktail (Roche) and incubated at 4 °C for 15 min. Cells were lysed by addition of 10% NP-40 (Sigma) before centrifuging at 4 °C and removal of the cytoplasmic extracts in the supernatant. The pellet was then resuspended in ice cold Buffer B (20 mM HEPES pH 7.9, 0.4 M NaCl, 1 mM EDTA, 1 mM EGTA, 1 mM DTT and 1 mM PMSF) containing protease inhibitors and vortexed vigorously for 45 min at 4 °C. Nuclear proteins were collected from supernatant following centrifugation at 4 °C. For all experiments three biological replicates were performed.

Invasion assay

Matrigel Matrix (Corning, 354230) was diluted to final concentration of 300 µg/mL in cold coating buffer (0.01 M Tris (pH8.0), 0.7% NaCl) before being added to invasion chambers (Corning Cat, 353097) and left to set overnight at 37 °C. 2×10^4 cells were added to each chamber in serum free medium and 0.75 mL complete medium was added to the wells. Cells were allowed to invade 24 h in cell culture incubator. Invading cells were fixed and permeabilised with 4% PFA (Electron Microscopy Sciences, 15713-S) and 0.1% Triton (Sigma). Non-Invading cells were removed using a cotton swab. Cells were stained with Crystal violet solution. For all experiments three technical and three biological replicates were performed.

Chromatin immunoprecipitation (ChIP)

ChIP was performed as previously described [39]. ChIP-PCR was performed using Quantitect SYBR green (Qiagen). The primers used can be found in Supplementary Table 1. For all experiments three biological replicates were performed.

CRIPSR-Cas9 mediated gene deletion

CBFβ and RUNX1 gene knockout was performed using a double nickase CRISPR-Cas9 strategy as described previously [31]. Guide-RNA sequences were designed using E-CRISP to minimise off target effects [24]. Cells were Fluorescence-activated cell sorted (FACS) for GFP-Cas9 expression 48 h after transfection and grown up from single colonies prior to genomic DNA PCR and western blot screening.

Mammary fat pad xenografts

3×10^6 MDA-MB-231 cells were transplanted in matrigel into the inguinal mammary fat pad of 12 week old *CD1-Nude* females (Charles River, UK). Mice were randomised to receive shNS or shCBFβ-KO cells to give groups of comparable weight/age. The same investigator (SMM) transplanted all cells into the recipients.

Animals were excluded if they failed to grow a tumour to clinical endpoint, and/or exhibited unrelated general ill health within the duration of the experiment.

Caliper measurements were carried out throughout by technical staff blinded to the expected outcome of the experiment to assess tumour volume which was calculated using the formula ½(length × width^2).

This experiment was carried out in dedicated animal facilities under project licence 60/4181 with adherence to the Animal (Scientific Procedures) Act, the European Directive 2010 and local ethical approval (University of Glasgow). No randomisation was required.

Bone tumour growth studies

Tumour growth studies used 6–8 week old female BALB/c nude between 13 and 18.4 g (Charles River, Kent, UK). Experiments were carried out in accordance with local guidelines and with Home Office approval under project licence 70/8799, University of Sheffield, UK. 12 mice per group were injected with 1×10^5 MDA-MB-231 control (2014-8-044) or CBFβ-CRISPR knockout cells (2015-6-010 CRISPR) via the left cardiac ventricle to generate tumours in bone [30]. Mice were randomised to receive control or CBFβ-KO cells to give groups of comparable weight/age. Mice were removed early from the study if they showed luciferase signal in the chest only (indicating a missed injection) or if the mice developed hind limb paralysis within the first 48 h. These parameters were predefined before the experiment commenced.

Animals were culled 26 days following tumour cell injection and hind limbs collected for analyses of tumour growth and associated bone lesions in tibiae and femurs.

Analysis of bone lesions

Hind limbs were fixed in 4%PFA and scanned by µCT prior to decalcification in 1%PFA/0.5% EDTA and processing for histological sectioning. µCT analysis was carried out using a Skyscan 1272 ×-ray-computed µCT scanner (Skyscan, Aartselar, Belgium) equipped with an x-ray tube (voltage, 50 kV; current, 200uA) and a 0.5-mm aluminium filter. Pixel size was set to 5.99 µm and scanning initiated from the top of the proximal tibia or distal femur. Lytic, tumour-induced bone lesions were counted manually for

each bone and performed by a technician being unaware of anticipated outcome of the experiment.

Statistical analysis

Data is represented as mean +/− SD, $n = 3$ unless otherwise stated.

Statistical significance was measured using parametric testing, assuming equal variance, unless otherwise stated, with standard *t*-tests for two paired samples used to assess difference between test and control samples. An asterisk (*) indicates $0.01 < P < 0.05$; ** indicates $0.001 < P < 0.01$; *** indicates $P < 0.001$; **** indicates $P < 0.0001$; *N* indicates $0.05 < P$ when compared to control.

Power calculations were performed for mammary fat pad experiments. Using 80% power and 95% confidence, 25% practical difference and 15% coefficient of variation we anticipated that 8-10 mice was required for each cohort and so $n = 10$ animals per cohort were transplanted.

Power calculations were also performed for bone tumour growth assays based on the minimum number of animals required to obtain statistically significant data in a factorial ANOVA design were based on our extensive previous studies: Metastasis is known to develop in the hind limbs of 80–90% of mice injected with control MDA-MB-231 cells, for studies predicted to decrease metastasis (or metastatic lesions) by 70%, a minimum of six mice per group is required to obtain 80% power with 10% error.

Acknowledgements The Bioimaging Facility microscopes used in this study were purchased with grants from BBSRC, Wellcome and the University of Manchester Strategic Fund. The FACS Aria within the flow cytometry core was purchased with funding from the MRC. We are grateful to Michael Jackson for guidance and assistance with cell sorting and to Anne Fowles for support with the in vivo studies of bone metastasis. Additional funding from The University Alumni Fund (RA) and CRUK (SM & KB (C596/A17196)). We would also like to thank the Core Services and Advanced Technologies at the Cancer Research UK Beatson Institute (C596/A17196), with particular thanks to Biological Services Unit and Histology.

Funding The work was funded by Breast Cancer Now (2013 May PR018; PS, IH and HH), a Cancer Research UK PhD Studentship (PS and HP), a BBSRC PhD studentship and the Manchester Alumni fund.

Author contributions RR performed most of the 3D and gene expression analysis of the knockdown cell lines and contributed to the development of the project. HH generated and analysed the CBFβ CRISPR cell line and contributed to the development of the project. RH performed the initial 3D analysis on CBFβ-knockdown cells. NSA generated and analysed the RUNX1 CRISPR cells. HP assisted with CRISPR and writing the manuscript. WD assisted with ChiP assays. PS performed the osteoblast co-cultures. AM assisted with the 3D bioreactor cultures. PO and SMM performed in vivo experiments. KB performed in vivo experiments and assisted with writing the manuscript. IH assisted with the conception and design of the project, interpretation of the data and preparation of the manuscript. PS conceived and directed the project and wrote the manuscript.

Compliance with ethical standards

Conflict of interest The authors declare that they have no conflict of interest.

Ethics approval All in vivo studies of bone metastasis were approved by the University of Sheffield project Applications and Amendments (Ethics) Committee and conducted in accordance with UK Home Office Regulations under project license 70/8799.

Publisher's note Springer Nature remains neutral with regard to jurisdictional claims in published maps and institutional affiliations.

References

1. Bianchini G, Balko JM, Mayer IA, Sanders ME, Gianni L. Triple-negative breast cancer: challenges and opportunities of a heterogeneous disease. Nat Rev Clin Oncol 2016;13:674–90.
2. Ferrari N, Mohammed ZM, Nixon C, Mason SM, Mallon E, McMillan DC, et al. Expression of RUNX1 correlates with poor patient prognosis in triple negative breast cancer. PLoS ONE. 2014;9:e100759.
3. McDonald L, Ferrari N, Terry A, Bell M, Mohammed ZM, Orange C, et al. RUNX2 correlates with subtype-specific breast cancer in a human tissue microarray, and ectopic expression of Runx2 perturbs differentiation in the mouse mammary gland. Dis Model Mech. 2014;7:525–34.
4. Rooney N, Riggio AI, Mendoza-Villanueva D, Shore P, Cameron ER, Blyth K. Runx genes in breast cancer and the mammary lineage. Adv Exp Med Biol. 2017;962:353–68.
5. Ito Y, Bae S-C, Chuang LSH. The RUNX family: developmental regulators in cancer. Nat Rev Cancer. 2015;15:81–95.
6. Tahirov TH, Bushweller J. Structure and biophysics of CBFβ/RUNX and its translocation products. Adv Exp Med Biol. 2017;962:21–31.
7. Ellis MJ, Ding L, Shen D, Luo J, Suman VJ, Wallis JW, et al. Whole-genome analysis informs breast cancer response to aromatase inhibition. Nature. 2012;486:353–60.
8. Banerji S, Cibulskis K, Rangel-Escareno C, Brown KK, Carter SL, Frederick AM, et al. Sequence analysis of mutations and translocations across breast cancer subtypes. Nature. 2012;486:405–9.
9. Shore P. A role for Runx2 in normal mammary gland and breast cancer bone metastasis. J Cell Biochem. 2005;96:484–9.
10. Pratap J, Lian JB, Stein GS. Metastatic bone disease: role of transcription factors and future targets. Bone. 2011;48:30–6.
11. Mendoza-Villanueva D, Deng W, Lopez-Camacho C, Shore P. The Runx transcriptional co-activator, CBFβ, is essential for invasion of breast cancer cells. Mol Cancer. 2010;9:171.
12. Mendoza-Villanueva D, Zeef L, Shore P. Metastatic breast cancer cells inhibit osteoblast differentiation through the Runx2/CBFβ-dependent expression of the Wnt antagonist, sclerostin. Breast Cancer Res. 2011;13:R106.

13. Kim DH, Xing T, Yang Z, Dudek R, Lu Q, Chen YH. Epithelial mesenchymal transition in embryonic development, tissue repair and cancer: a comprehensive overview. J Clin Med. 2017;7:1.
14. Chaffer CL, San Juan BP, Lim E, Weinberg RA. EMT, cell plasticity and metastasis. Cancer Metastasis Rev. 2016;35:645–54.
15. Ingthorsson S, Briem E, Bergthorsson JT, Gudjonsson T. Epithelial plasticity during human breast morphogenesis and cancer progression. J Mammary Gland Biol Neoplasia. 2016;21:139–48.
16. Ye X, Tam WL, Shibue T, Kaygusuz Y, Reinhardt F, Ng Eaton E, et al. Distinct EMT programs control normal mammary stem cells and tumour-initiating cells. Nature. 2015;525:256–60.
17. Luo M, Brooks M, Wicha MS. Epithelial-mesenchymal plasticity of breast cancer stem cells: implications for metastasis and therapeutic resistance. Curr Pharm Des. 2015;21:1301–10.
18. Chimge NO, Baniwal SK, Little GH, Chen YB, Kahn M, Tripathy D, et al. Regulation of breast cancer metastasis by Runx2 and estrogen signaling: the role of SNAI2. Breast Cancer Res. 2011;13:R127.
19. Chimge N-O, Frenkel B. The RUNX family in breast cancer: relationships with estrogen signaling. Oncogene. 2013;32:2121–30.
20. Kulkarni M, Tan TZ, Syed Sulaiman NB, Lamar JM, Bansal P, Cui J, et al. RUNX1 and RUNX3 protect against YAP-mediated EMT, stem-ness and shorter survival outcomes in breast cancer. Oncotarget. 2018;9:14175–92.
21. Browne G, Taipaleenmäki H, Bishop NM, Madasu SC, Shaw LM, van Wijnen AJ, et al. Runx1 is associated with breast cancer progression in MMTV-PyMT transgenic mice and its depletion in vitro inhibits migration and invasion. J Cell Physiol. 2015;230:2522–32.
22. Pratap J, Imbalzano KM, Underwood JM, Cohet N, Gokul K, Akech J, et al. Ectopic runx2 expression in mammary epithelial cells disrupts formation of normal acini structure: implications for breast cancer progression. Cancer Res. 2009;69, 6807–14.
23. Kenny PA, Lee GY, Myers CA, Neve RM, Semeiks JR, Spellman PT, et al. The morphologies of breast cancer cell lines in three-dimensional assays correlate with their profiles of gene expression. Mol Oncol. 2007;1:84–96.
24. Debnath J, Muthuswamy SK, Brugge JS. Morphogenesis and oncogenesis of MCF-10A mammary epithelial acini grown in three-dimensional basement membrane cultures. Methods. 2003;30:256–68.
25. Harrison H, Farnie G, Howell SJ, Rock RE, Stylianou S, Brennan KR, et al. Regulation of breast cancer stem cell activity by signaling through the Notch4 receptor. Cancer Res. 2010;70:709–18.
26. Zhu Y, Luo M, Brooks M, Clouthier SG, Wicha MS. Biological and clinical significance of cancer stem cell plasticity. Clin Transl Med. 2014;3:32.
27. Shore P, Dietrich W, Corcoran LM. Oct-2 regulates CD36 gene expression via a consensus octamer, which excludes the co-activator OBF-1. Nucleic Acids Res. 2002;30:1767–73.
28. Ferrari N, Riggio AI, Mason S, McDonald L, King A, Higgins T, et al. Runx2 contributes to the regenerative potential of the mammary epithelium. Sci Rep. 2015;5:15658.
29. Mastro AM, Vogler EA. A three-dimensional osteogenic tissue model for the study of metastatic tumor cell interactions with bone. Cancer Res. 2009;69:4097–100.
30. Holen I, Lefley DV, Francis SE, Rennicks S, Bradbury S, Coleman RE, et al. IL-1 drives breast cancer growth and bone metastasis in vivo. Oncotarget. 2016;7:75571–84.
31. Ran FA, Hsu PD, Wright J, Agarwala V, Scott DA, Zhang F. Genome engineering using the CRISPR-Cas9 system. Nat Protoc. 2013;8:2281–308.
32. Prat A, Parker JS, Karginova O, Fan C, Livasy C, Herschkowitz JI, et al. Phenotypic and molecular characterization of the claudin-low intrinsic subtype of breast cancer. Breast Cancer Res 2010;12:R68.
33. Chimge N-O, Ahmed-Alnassar S, Frenkel B. Relationship between RUNX1 and AXIN1 in ER-negative versus ER-positive Breast Cancer. Cell Cycle. 2017;16:312–8.
34. van Bragt MP, Hu X, Xie Y, Li Z. RUNX1, a transcription factor mutated in breast cancer, controls the fate of ER-positive mammary luminal cells. Elife. 2014;3:e03881.
35. Browne G, Dragon JA, Hong D, Messier TL, Gordon JA, Farina NH, et al. MicroRNA-378-mediated suppression of Runx1 alleviates the aggressive phenotype of triple-negative MDA-MB-231 human breast cancer cells. Tumour Biol. 2016;37:8825–39.
36. Hong D, Messier TL, Tye CE, Dobson JR, Fritz AJ, Sikora KR, et al. Runx1 stabilizes the mammary epithelial cell phenotype and prevents epithelial to mesenchymal transition. Oncotarget. 2017;8:17610–27.
37. Illendula A, Gilmour J, Grembecka J, Tirumala VSS, Boulton A, Kuntimaddi A, et al. Small molecule inhibitor of CBFβ-RUNX binding for RUNX transcription factor driven cancers. EBioMed. 2016;8:117–31.
38. Shaw FL, Harrison H, Spence K, Ablett MP, Simões BM, Farnie G, et al. A detailed mammosphere assay protocol for the quantification of breast stem cell activity. J Mammary Gland Biol Neoplasia. 2012;17:111–7.
39. Deng W, Lopez-Camacho C, Tang JY, Mendoza-Villanueva D, Maya-Mendoza A, Jackson DA, et al. Cytoskeletal protein filamin A is a nucleolar protein that suppresses ribosomal RNA gene transcription. Proc Natl Acad Sci 2012;109:1524–9.